REPORT DOCUMENTATION PAGE

Form Approved
OMB No. 0704-0188

1a. REPORT SECURITY CLASSIFICATION Unclassified	1b. RESTRICTIVE MARKINGS None
2a. SECURITY CLASSIFICATION AUTHORITY	3. DISTRIBUTION / AVAILABILITY OF REPORT Approved for public release; distribution unlimited
2b. DECLASSIFICATION / DOWNGRADING SCHEDULE	
4. PERFORMING ORGANIZATION REPORT NUMBER(S) UILU-ENG-94-2212	5. MONITORING ORGANIZATION REPORT NUMBER(S)
6a. NAME OF PERFORMING ORGANIZATION Coordinated Science Lab. University of Illinois 6b. OFFICE SYMBOL (If applicable)	7a. NAME OF MONITORING ORGANIZATION
6c. ADDRESS (City, State, and ZIP Code)	7b. ADDRESS (City, State, and ZIP Code)
8a. NAME OF FUNDING / SPONSORING ORGANIZATION 8b. OFFICE SYMBOL (If applicable)	9. PROCUREMENT INSTRUMENT IDENTIFICATION NUMBER
8c. ADDRESS (City, State, and ZIP Code)	10. SOURCE OF FUNDING NUMBERS PROGRAM ELEMENT NO. / PROJECT NO. / TASK NO. / WORK UNIT ACCESSION NO.

11. TITLE (Include Security Classification)

SHAPE MATCHING BY ELASTIC DEFORMATION

12. PERSONAL AUTHOR(S)
Simone Santini, Jorge Sanz, Alberto Del Bimbo

13a. TYPE OF REPORT	13b. TIME COVERED	14. DATE OF REPORT (Year, Month, Day)	15. PAGE COUNT
Technical	FROM _____ TO _____	1994 March 15	25

16. SUPPLEMENTARY NOTATION

17. COSATI CODES			18. SUBJECT TERMS (Continue on reverse if necessary and identify by block number)
FIELD	GROUP	SUB-GROUP	shape matching, elastic deformation, template

19. ABSTRACT (Continue on reverse if necessary and identify by block number)

In this paper we present a new one-dimensional shape matching technique based on elastic deformation of a model or template. Deformations of the given template are introduced as a way to improve the matching with the image data. A trade-off is made between the amount of deformation and a figure of merit that accounts for the match. This approach yields a new optimization functional so that the optimal match for a given shape is expressed as a solution of a variational problem. Numerical methods are presented to solve the resulting system of ordinary differential equations.

This new matching technique can be used for pattern recognition applications where binarizing images is hard or impossible. An illustration of the new shape matching method is shown for several optical character recognition problems.

20. DISTRIBUTION / AVAILABILITY OF ABSTRACT ☒ UNCLASSIFIED/UNLIMITED ☐ SAME AS RPT. ☐ DTIC USERS	21. ABSTRACT SECURITY CLASSIFICATION Unclassified
22a. NAME OF RESPONSIBLE INDIVIDUAL	22b. TELEPHONE (Include Area Code) / 22c. OFFICE SYMBOL

March 1994 UILU-ENG-94-2212

SHAPE MATCHING BY ELASTIC DEFORMATION

Simone Santini
Jorge Sanz
Alberto Del Bimbo

Coordinated Science Laboratory
College of Engineering
UNIVERSITY OF ILLINOIS AT URBANA-CHAMPAIGN

Shape Matching by Elastic Deformation

[1]Simone Santini [2]Jorge Sanz [3]Alberto Del Bimbo

1, 2 - Department of Electrical and Computer Engineering,
The University of Illinois at Urbana-Champaign

3 - University of Florence, Italy

Abstract

In this paper we present a new one-dimensional shape matching technique based on elastic deformation of a model or template. Deformations of the given template are introduced as a way to improve the matching with the image data. A trade-off is made between the amount of deformation and a figure of merit that accounts for the match. This approach yields a new optimization functional so that the optimal match for a given shape is expressed as a solution of a variational problem. Numerical methods are presented to solve the resulting system of ordinary differential equations.

This new matching technique can be used for pattern recognition applications where binarizing images s hard or impossible. An illustration of the nre shape matching method is shown for several optical character recognition problems.

1 Introduction

In this paper, we present a new shape matching technique based on the deformation of a one-dimensional "sketch" of the shape to be matched. The sketch (or *template*) can be visualized as made up of an elastic material, and is deformed to find the best possible match in the image.

The new technique is a generalized form of template matching in which a model of the shape is known in advanced and the image is searched for evidence supporting the presence of the model. Traditional template matching techniques are quite inflexible and sensitive to small geometrical distortion of the sought pattern. In our method, deformations of the pattern are allowed as a way to improve the matching with the image data. A trade-off is made between the amount of deformation in the pattern and a figure of merit that accounts for the match.

Shape matching methods can be classified according to the way apriori knowledge of the shape is used. In *data-to-model* methods, raw image data is analyzed by extracting features and comparing them to those rendered by the model.

On the contrary, in *model-to-data* methods, such as template matching, we start with a model (the *template*), and search the image for evidence supporting the presence of the model. This is essentially a top-down procedure and, in principle, it could give better results than data-to-model methods, since it can use a priori information embedded in the model that feature extraction-based methods cannot exploit.

The technique presented in this paper belongs to the general class of model-to-data methods. As an illustration of the significant improvements that the new technique introduces over template matching, we will analyze its advantages in two scenarios.

The two most common applications of a template matching technique are *similarity ranking* and *class assignment.* Similarity ranking is carried out when looking for an image in an image database based on the sketch of a shape. In this case, we have one template, and a number of images. The goal is to rank the images according to their similarity with the template. The effect of brittle matching in this case is to narrow the scope of the search: only images with shapes very similar to the template are ranked well. Other images in the data base containing deformed ocurrences of the sought shape may receive meaningless scoring.

In class assignment, a series of different templates representing *classes* are matched against a single image. The class of the template with the best match is sought. An example of class assigment is optical character recognition. In this case, the effect of brittle matching is the proliferation of templates. For instance, in [6], template matching is used for the recognition of digits. In that case, 1,000 templates are used to recognize a training set of 10,000 digits with 95% accuracy. This large number of templates was necessary to take into account all the variations of the digits in the training set. This will also pose problems for the recognition of digits that are not part of the training set: there is no warrantee that other digits with different distortion than those in the training set will be recognized by the same templates.

We believe that reliable figures of merit or similarity measures for matching can be

obtained from the elastic deformation energy of a prototype shape. This gives a template a great flexibility in matching similar shapes, and provides graceful degradation of the similarity measure as the two shapes to be matched are set apart.

One can picture the technique by thinking of a thin metallic bar, that is melted in a furnace and given the shape of the template. In the matching process, the bar starts by assumeing the shape of the template without internal stress, that is, in a status of minimal internal energy. Then, we start stretching and bending the bar, trying to adapt it to the relevant characteristics of the image[1]. While doing this, we simultaneously keep track of the degree to which the deformed bar matches the image, and of the deformation energy of the bar, looking for a "good compromise" between the two.

The outline of the paper is as follows. In Section 2, we briefly discuss related work. In Section 3, the new matching technique is presented. The properties of the optimal deformation of the template are studied in Section 4. In Section 5, the numerical solution to the shape matching problem is described. Different possible measures of the quality of match are discussed in section 6. Also in section 6, the variation of these measures with respecto to the initial position of the template is studied. Section 7 shows a new approach to an OCR problem where conventional binarization of digits is impossible. This OCR approach is obtained by using the shape matching technique shown in the paper.

2 Related Work

In the past, researchers have developed a number of techniques for shape matching based on deformation and continuity. In this section we briefly review these techniques, and highlight the differences with respect to our method.

The most widely known objects with elastic deformation properties are the *snakes* [8, 15, 19]. A snake is a spline curve that is superimposed to an image, and deformed to match image contours, while retaining certain smoothness characteristics. Snakes have been used mainly for extraction of smooth boundaries and applied, e.g. to head boundaries identification [19].

The main difference between snakes and the approach presented in this paper is that snakes carry no *a priori* model of the shape. Rather, "smooth" contours are sought. This makes the snakes not well suited to look for contours that are not smooth. Actually, in some papers (e.g. [15]), it was noted that snakes do not give satisfactory results when requested to look for a rectangle in the image, because the smoothness requirements cannot be met at the sharp corners.

In our approach, on the contrary, we have a model that, however irregular it may be, represents the state of zero energy, and we set constraints only on the deformation of the original model. Therefore, looking for a rectangle, or for any irregular shape is not –

[1]The relevant characteristics depend heavily on the application, and the issue will be given the proper mathematical treatment in the following sections. For the present example, we can assume that the template is fitted to the edges of the image.

given the appropriate model – different from looking for a circle or for any very regular shape.

To emphasise the difference by means of a physical analogy, we could stress that, in the snakes model, a rubber band – whose undeformed state is a very small ring – is extended to fit edges in the image.

In our approach, on the contrary, a rubber sheet with shape of the sought template is deformed to match the image data.

Another approach has been proposed that models digits in an OCR application as splines [7, 20]. The model is then fitted to a binary image of a digit, and the agreement between the model and the image is measured by the displacement that it is necessary to give to the original control points to obtain the maximum match.

This method suffers from the same drawbacks as the snakes. Namely, it cannot easily fit shapes that cannot be modeled as a smooth spline. In addition, it uses an optimization procedure that maximizes the probability that all pixels be generated by the spline. As such, it is not easily generalizable to deal with gray level images.

Other methods have been proposed to impose continuity and smoothness constraints on deformation directly on the discrete images.

For instance, Burr [2] proposes a method to *register* images, that is, to find point corresponcencs between two images. The goal is to find one-to-one associations between points in the first image and corresponding (displaced) points in the second image. At first, every point in the undeformedimage makes a tentative match with a point in the deformed image. In general, many of these point relations will be wrong. To correct them, Burr uses a relaxation process, based on constraints between nearby points. The constraint is basically that nearby points in the undeformed image should be connected to nearby points in the deformed image. This relaxation process eventually leads to the right registration.

Methods similar to Burr's find application in OCR [17], and in shape matching [3].

3 The Matching Technique

The model in our approach is a one-dimensional template $\tau : \mathbb{R} \mapsto \mathbb{R}^2$, which is a curve in the image space, parametrized with respect to the arc length s. All the curves we use have length normalized to 1. The individual components of τ will be denoted by τ^μ, where greek indeces take values in $\{1, 2\}$. Einstein's summation convention will be used throughout the paper. Also, let $\beta : \mathbb{R}^2 \mapsto [0, 1]$ be the image to be fit with the template.

Since the exact shape of τ will not be present, in general in the image, deformations of the original template τ have to be allowed to find a good match with the image data.

Thus, the deformation θ is a unitary length smooth curve $\theta : [0, 1] \mapsto \mathbb{R}^2$, which is added pointwise to the model template τ so as to obtain the deformed template

$$\phi(s) = \tau(s) + \theta(s)$$

In terms of the analogy outlined in the introduction, we can say that τ is the mold used in the furnace to melt the prototype: the "original" shape of the template. On the

other hand, ϕ is the metallic bar that can be made different from τ due to the deformation θ.

To measure how far we go from τ, we measure the elastic energy of the deformation. This energy is computed based on the deformation $\theta(s)$ as:

$$\int_0^1 \left\{ \alpha^1 \left[\left(\frac{d\theta^1}{ds} \right)^2 + \left(\frac{d\theta^2}{ds} \right)^2 \right] + \alpha^2 \left[\left(\frac{d^2\theta^1}{ds^2} \right)^2 + \left(\frac{d^2\theta^2}{ds^2} \right)^2 \right] \right\} ds \tag{1}$$

To ease the notation, we set:

$$\theta^\mu_{,j} = \frac{d^j \theta^\mu}{ds^j} \quad \mu = 1, 2 \tag{2}$$

so that eq. (1) becomes:

$$\int_0^1 \alpha^i \left(\theta^\mu_{,i} \theta^\sigma_{,i} \delta_{\mu\sigma} \right) ds \tag{3}$$

Note that in eq. (3) the measured elastic energy is that of the *deformation*. It doesn't matter how irregular, even discontinuous, the shape of the template τ might be. Taking back the physical analogy, when the metallic bar has been melted in a given shape, it takes that shape without internal tensions, no matter how irregular it is. Only when the shape is modified by θ a state of stress appears.

In addition to the deformation, we want to know how well the deformed template ϕ fits the image β. The way this measure is defined depends in part on the nature of the application.

Foe example, if the shape we are fitting is a drawing in the image plane (as could be the case of OCR), then we have to fit the template to the "black" areas of the image.

If $\beta(x)$ representes the "blackness" at point x, then a measure of the fitness between the elastic template ϕ and the image is given by:

$$\int_0^1 [\beta(\phi(s))]^r \, ds \tag{4}$$

Where $r > 0$ is a "shape factor" coefficient that can be used to weigh the match in "almost black" areas differently from the match in "almost white" areas. For instance, if $\beta \in [0, 1]$, as will be assumed henceforth, when $r \to \infty$, only areas in which $\beta = 1$ give a contribution to the integral, while all the areas in which β is grey do not contribute.

On the other hand, if we look for a particular shape in a general image (e.g. the shape of a car in an outdoor scene), then we want to fit the template against the *contours* of the image. A way to do this is to place the template on the maxima of the gradient of the image. In this case, the match measure could be:

$$\int_0^1 [|\nabla \beta(\phi(s))|]^r \, ds \tag{5}$$

where r has the same meaning as in (4).

For the general case, assume a differential operator is given:

$$D_M = a_0 + \sum_{r_1+r_2<=N} a_{r_1 r_2} \frac{\partial}{\partial x_1^{r_1} \partial x_2^{r_2}} \tag{6}$$

and let $\Psi(x)$ be defined as:

$$\Psi[x] = \|D_M \beta(x)\|^r \tag{7}$$

Then, the matching term can be expressed as:

$$\int_0^1 \Psi\left[\phi(s)\right] ds \tag{8}$$

Note that the two cases in (4) and (5) above can be obtained as special cases of (8) by setting $a_0 = 1$, $a_{ij} = 0$, for the "blackness" matching and $a_{10} = a_{01} = 1$, $a_{ij} = 0$ otherwise for the contour matching.

The elastic template should find a compromise between the maximization of eq. (8), which measures the match between the deformed template and the image, and the minimization of eq. (3), which measures the deformation of the template from its original position. This compromise is accomplished by minimizing the compound expression:

$$\int \Phi(\theta) = \int_0^1 \left\{ \alpha^i \left(\theta^\mu_{,i} \theta^\sigma_{,i} \delta_{\mu\sigma} \right) - \Psi\left[\phi(s)\right] \right\} ds \tag{9}$$

This is a regularization problem of the type discussed in [16], whose solution is obtained by variational techniques [9], and where the function

$$\Phi(\theta) = \alpha^i \left(\theta^\mu_{,i} \theta^\sigma_{,i} \delta_{\mu\sigma} \right) - \Psi\left[\phi(s)\right] \tag{10}$$

plays the role of a Lagrangian function.

Writing down the Euler-Lagrange equations for this problem, we have:

$$\alpha^2 \theta^\mu_{,4} - \alpha^1 \theta^\mu_{,2} = \frac{\partial}{\partial \theta^\mu} \left(\Psi\left[x\right] \right) \Big|_{(\theta+\tau)(s)} \tag{11}$$

working out the derivatives and the summations, the system of ordinary differential equations to be solved is:

$$\alpha^2 \frac{d^4 \theta^\mu}{ds^4} - \alpha^1 \frac{d^2 \theta^\mu}{ds^2} = \frac{\partial \Psi[x]}{\partial \theta^\mu} \Big|_{(\theta+\tau)(s)}, \quad \mu = 1, 2. \tag{12}$$

Solving this system of equations gives the deformation θ that minimizes $\int \Phi$, thus, the deformation that optimally fits τ to the image β.

4 Solution of the Variational Problem

The problem posed in the previous paragraph is a regularization problem in the sense of Tihonov [16, 13], whose solution requires the integration of the system of nonlinear

ordinary differential equations (11). The solution of the problem in closed form is in general impossible, and a suitable numerical technique has to be used for the solution.

In this section, we study the solution to the variational problem (9) and show that if we approximate the integral $\int \Psi$ by a summation taken over n points, then a locally optimal solution can be found in a space of dimension n. This means that there are n functions $g_1, \ldots, g_n$ such that the locally optimal solution is given by:

$$f = \sum_{i=1}^{n} \mu_i g_i$$

for some suitable coefficients μ_i. This property is important since it allows to reduce the differential equation (11) to an algebraic system in $2n$ unknown (n coefficients μ_i for each component of the deformation θ).

Our proof is an extension of that in [18] in which it has been proven that a similar property holds when Ψ is linear in ψ.

If we approximate the integral with a summation taken over n points, the second term in the variational problem (9) becomes:

$$\sum_{i=1}^{n} [\Psi[\phi(s_i)]] . \tag{13}$$

This is the quantity that the variational equation tries to maximize. If we assume that Ψ is limited by M, the maximization of (8) is tantamount to the minimization of:

$$\sum_{i=1}^{n} [M - \Psi[\phi(s_i)]] \tag{14}$$

or, since $0 \leq \Psi \leq M$, to the minimization of:

$$\sum_{i=1}^{n} [M - \Psi[\phi(s_i)]]^2 . \tag{15}$$

The variational problem (9) can thus be restated as:

$$\delta \left\{ \|D_S \phi\|^2 + \sum_{i=1}^{n} [M - \Psi(\phi(s_i))]^2 \right\} = 0 \tag{16}$$

with

$$D_S = \alpha^1 \frac{d}{ds} + \alpha^2 \frac{d^2}{ds^2} \tag{17}$$

In this section, we discuss how the results of [1] can be extended to the present case under the hypothesis of "small" displacement of the spline from the optimal solution.

We start by posing the problem in a quite general and abstract form, which contains the variational problem (16) as a special case.

Let X and Y be real Hilbert spaces and $D \in \mathcal{L}[X, Y]$, the space of linear operators on X into Y. Define the kernel $\mathcal{N}$ of a generic transformation F as:

$$\mathcal{N}(F) = \{x \in X | F(x) = 0_Y\} \tag{18}$$

and the range as

$$\mathcal{R}(F) = \{y \in Y | \exists x \in X : F(x) = y\} \tag{19}$$

Let n functionals $k_i : X \mapsto \mathbb{R}$ be given, define $A : X \mapsto \mathbb{R}^n$ as $A(x) = [k_1(f), \ldots k_n(f)]$ with $f \in X$, and let $\bar{r} \in \mathbb{R}^n$ be given. We call *smoothing spline function* relative to D, A and $\bar{r}$ any element $s \in X$ that satisfies:

$$\|L(s)\|^2 = \min_{f \in X} \|L(f) - r\|^2. \tag{20}$$

with $L : X \mapsto Z = \mathbb{R}^n \times Y$ defined as:

$$L(f) = [k_1(f), \ldots k_n(f)\,;\, Df] \tag{21}$$

and

$$r = [\bar{r}; 0] = [r_1, \ldots r_n; 0_Y] \tag{22}$$

The norm in Z is defined as:

$$\|L(f) - r\|^2 = \rho \sum_{i=1}^{n} (k_i(f) - r_i)^2 + \|Df\|_Y^2 \tag{23}$$

where $\|\cdot\|_Y$ is the norm induced by the inner product in Y.

Z is an infinite dimensional Euclidean space, and $Q = LX$ is a manifold embedded in Z. Note that the immersion of X in Y defined by the second part of L is linear, while the immension of X into the finite dimensional space $\mathbb{R}^n$ defined by the first n components of L is nonlinear.

Let TQ be the tangent bundle of Q. For every $\chi \in Q$, $T_\chi Q$ is a linear space, isomorphic to a linear subspace of Z. If $T_\chi^\perp Q$ is the subspace orthogonal to $T_\chi Q$, then

$$Z = T_\chi Q \oplus T_\chi^\perp Q \tag{24}$$

Note that all these spaces are euclidean, and thus they are isomorphic to their tangent spaces. For the sake of clarity we will distinguish, when needed, from the element $s \in LX$ and the same element thought as belonging to Z. To this end, we introduce the natural immersion $\iota : LX \mapsto Z$.

Theorem 4.1 *A function $s \in X$ is an extremum of the variational problem $\delta\|L(s) - r\|^2 = 0$ iff*

$$\iota(L(s) - r) \in T_{L(s)}^\perp Q \tag{25}$$

Proof:
the proof is by contraddiction. Suppose $\iota(L(s) - r) = \gamma + p$, with $p \in T_{L(s)}^\perp Q$ and $\gamma \in T_{L(s)}^\perp Q$. Consider a curve $q : [-1, 1] \mapsto Q$, with $q(0) = L(s)$ and $\dot{q}(0) = \gamma$. Set $d(t) = \|q(t) - r\|^2$.

In this case, we have:

$$\dot{d}(t) = -2\langle q(t) - r, \dot{q}(t)\rangle_Z$$

and:

$$\dot{d}(0) = -2\langle q(0) - r, \dot{q}(0)\rangle_Z = -2\langle(\gamma + p), \gamma\rangle_Z$$

Since γ and p are orthogonal, it holds:

$$\dot{d}(0) = -2\|\gamma\|^2 < 0$$

Therefore, $\|L(s) - r\|^2$ cannot have an extremum along the curve q at $t = 0$. Since s is an extremum in LX if and only if it is an extremum along all the curves in LX that pass through it, this proves the theorem □

Considering the function $L : X \mapsto Z$, we can build the differential $L_* : T_sX \mapsto T_{L(s)}Z$ and the pull-back $L^* : T^*_{L(s)}Z \mapsto T^*_sX$ (see [12]). Note that, since X and Z are euclidean – and hence isomorphic to their tangent spaces – we can write:

$$L_* : X \mapsto Z$$

and

$$L^* : Z \mapsto X$$

in a similar way we can define D_*, D^*, A_*, and A^*. Note that, once a point $s \in X$ has been set, all these are linear transformations.

Moreover, set $N = \mathcal{N}(D_*)$ and $q = \dim\ N$.

Before we prove the main theorems, we report the following lemma from [18]:

Lemma 4.1 *Let M be any subspace of X, and $F : X \mapsto Y$, then*

$$F^*(F_*M)^\perp = \mathcal{R}(F^*) \cap M^\perp \tag{26}$$

Proof:
Let $y \in Y$. Then, by (30), $y \in (F_*M)^\perp$ if and only if $F^*y \in M^\perp$. This also implies $y \in \mathcal{R}(F^*)$.

Thus, in $\mathcal{R}(F^*)$, we can write $(F_*M)^\perp = (F^*)^{-1}M^\perp$. Restricting this equality to $\mathcal{R}(F^*)$, and applying F^* to both sides yields eq. (26). □

Theorem 4.2 *For every point $\chi \in Q$ we have:*

$$T^\perp_\chi Q = G \tag{27}$$

with:

$$G = \mathcal{N}(L^*) \tag{28}$$

$$\dim\ G = n - q \tag{29}$$

Proof:
We first prove (28).

From the definition of the differential and the pull-back, it results, for any function $\Psi : M \mapsto U$, where M and U are arbitrary manifolds, and $v \in TM$, $\omega \in T^*U$ ([12]) it holds

$$\langle \omega, \Psi_* v \rangle_U = \langle \Psi^* \omega, v \rangle_M \tag{30}$$

From (30) is easy to show that:

$$T_\chi Q = \mathcal{R}(L_*) = \mathcal{N}(L^*)^\perp \tag{31}$$

where L_* and L^* are to be computed at the point χ. From this follows that:

$$T_{\dot{\chi}}^\perp Q = \mathcal{N}(L^*).$$

To prove (29), let $z = [z_Y, z_E] \in Z$. Since Y and E are euclidean, it is also $z_Y \in T_z Y$ and $z_E \in T_z E$, thus we can write

$$L^* z = D^* z_Y + \rho A^* z_E$$

To have $z \in \mathcal{N}(L^*)$, we must have $L^* z = 0$, that is, there must be x such that

$$x = D^* z_Y = -\rho A^* z_E$$

that is:

$$\begin{aligned} x \in D^*Y \cap A^*E &= \mathcal{R}(D^*) \cap \mathcal{R}(A^*) \\ &= \mathcal{N}(D_*)^\perp \cap \mathcal{R}(A^*) \\ &= \mathcal{R}(A^*) \cap N^\perp \\ &\stackrel{\text{def}}{=} H \end{aligned}$$

By lemma 4.1,

$$H = \mathcal{R}(A^*) \cap N^\perp = A^*(A_* N) \tag{32}$$

but, since dim $A_* N =$ dim $N = q$, we have (being T^* and A^* one-to-one):

$$\text{dim } A^*(A_* N) = \text{dim } G = n - q$$

□

We can build a basis for H in the following way. Set $B = (AN)^\perp$, and let $\{b_1, \ldots b_{n-q}\}$ be a basis for B, then, from eq. (32), it follows that a basis for H is given by $\{h_1, \ldots h_{n-q}\}$, with $h_i = A^* b_i$.

With the basis for H, noting that $L^* G = H$ and that L^* is invertible over H, we can build a basis for G as $\{g_1, \ldots g_{n-q}\}$ with

$$g_i = \left[T^{*-1} h_i, \frac{A^{*-1} h_i}{\rho} \right] \tag{33}$$

Theorem 4.3 *The solution of the minimization problem (20) is the element $s \in X$ such that:*

$$L(s) - r = \sum_{j=1}^{n-q} \mu_j g_j \in G \tag{34}$$

where the μ_i satisfy the algebraic system:

$$\sum_{j=1}^{n-q} \mu_j \langle g_j, g_i \rangle_Z = -\langle a, g_i \rangle_Z \quad i = 1, \ldots n-q. \tag{35}$$

Proof:
This theorem is proved, for the smoothing spline, in ([1]). We repeat here the proof using our symbolism, for the sake of clarity.

By eqs. (25) and (27), we have $L(s) - a \in G$, thus (34) holds.

Also, since $L(s) \in LX = Q$, we have, from eq. (27), $L_*(s) \in G^\perp$, thus:

$$L_* s = \sum_{j=1}^{n-q} \mu_j g_j + r \in G^\perp \tag{36}$$

thus the inner product of L_* with any element of the basis of G, g_i, vanishes: $\langle L_* s, g_i \rangle_Z = 0$. Expressing L_* as in eq. (36) yields (35). □

We can apply these theorems to the case of the elastic deformation by setting $n = 1$, and:

$$\begin{aligned} k_1(\theta) &\stackrel{\text{def}}{\equiv} \Psi[\phi(s)] \\ r &\stackrel{\text{def}}{\equiv} [M; 0] \\ D &= D_S \end{aligned} \tag{37}$$

where D_S is the differential operator of the variational problem resulting from the elastic deformation, as defined in (17).

5 Numerical Solution

The spline solution discussed in the previous section makes it possible to reduce the differential variational problem of Sect. 3 to an algebraic nonlinear problem in which the control points of the spline function describing the deformation θ are the unknowns.

The number of knots of θ determine the computational complexity of the problem and, by means of the approximation (13), it also determines the degree by which the variational problem (16) that we solve by means of a spline function approximates the true elasticity variational problem (9).

The situation is different for the original template τ. The template τ is not involved in the solution of the variational problem but in the evaluation of

$$\left. \frac{\partial \Psi}{\partial \theta^\nu} \right|_{\tau + \theta}.$$

The numerical complexity of the problem is therefore independent on the number of points we use to describe the template.

On the other side, we want a description of the shape τ that allows for shape irregularities, without imposing any artificial smothness constraint. This can be accomplished by using a piecewise linear approximation for the template: the linear approximation can accomodate sharp corners, and, since the template is known exactly a priori, it can be made as precide as desired by using a suitable number of knots.

According to this, the template τ is represented by a set of N_τ points

$$T = \left\{(\tau_\lambda^1, \tau_\lambda^2), \lambda = 0 \dots N_\tau\right\} \tag{38}$$

which are supposed equidistant in the interval $[0,1]$. That is, the point $(\tau_\lambda^1, \tau_\lambda^2)$ is the value assumed by the prototype $\tau(s)$ for $s = s_\lambda = \lambda/N_\tau$. The value of the prototype at the point s can be computed by the linear interpolation equation: given by

$$\tau(s) \stackrel{\text{def}}{\equiv} \begin{bmatrix} \tau^1_{\lfloor N_\tau s \rfloor} + (N_\tau s - \lfloor N_\tau s \rfloor)\left(\tau^1_{\lfloor N_\tau s \rfloor + 1} - \tau^1_{\lfloor N_\tau s \rfloor}\right) \\ \tau^2_{\lfloor N_\tau s \rfloor} + (N_\tau s - \lfloor N_\tau s \rfloor)\left(\tau^2_{\lfloor N_\tau s \rfloor + 1} - \tau^2_{\lfloor N_\tau s \rfloor}\right) \end{bmatrix} \tag{39}$$

For the deformation θ, we have to take into account the smoothness constraints: θ results as the solution of eq. (11), which is a fourth order differential equation. This means that we must guarantee the existence at least of the fourth derivative of θ.

We guarantee the required continuity degree representing θ by fifth order splines. Let $B_\nu^{(5)}$ be the ν-th element of the B-spline basis of the space of fifth order splines with equidistant knots. We divide the interval $[0,1]$ into N_θ interval by selecting the knots $s_\nu = \nu/N_\theta$, with $\nu = 0 \dots N_\theta$.

We add three "ghost" knots on each side of the interval (these knots are used to build some of the B-spline that assume nonzero values in the extreme knots; see [14]), so that the full set of knots is:

$$\left\{s_\nu = \frac{\nu}{N_\theta}; \nu = -3 \dots N_\theta + 3\right\} \tag{40}$$

The deformation θ in the point $s \in [0,1]$ can then be expressed as:

$$\theta(s) = \sum_{\nu=-3}^{N_\theta+3} \begin{bmatrix} c_\nu^1 \\ c_\nu^2 \end{bmatrix} B_\nu^{(5)}(s) \tag{41}$$

The coefficients c_ν^μ, $\nu = -3 \dots N_\theta + 3$, $\mu = 1,2$ determine the solution uniquely. The solution can thus be found by imposing eq. (11) in all the knots.

At the ν-th knot we have:

$$\theta_{,j}^\mu(s_\eta, \mathbf{c}) = \sum_{\nu=\eta-3}^{\eta+3} c_\eta^\mu B_{\nu\ ,j}^{(5)}(s_\eta) \tag{42}$$

where

$$\begin{aligned} \mathbf{c} &= \{c_{\nu\mu}\} \\ &= \{c_\nu^\mu\},\ \nu = -3 \dots N_\theta + 3\ \mu = 1,2 \end{aligned} \tag{43}$$

(that is, $c \in \mathbb{R}^{(N_\theta+6)\times 2}$). The range in which the index ν varies depends on the fact that the B-splines have compact support so that, given a knot s_η only a limited number of B-splines assume there nonzero values.

Equation (11) can be written in the knot s_η as:

$$\sum_{\nu=\eta-3}^{\eta+3} \left[\alpha^2 B_\nu^{(5)}{}_{,4}(s_\eta) - \alpha^1 B_\nu^{(5)}{}_{,2}(s_\eta)\right] c_\nu^\mu = \left.\frac{\partial \mu}{\partial \theta^\mu}\right|_{\theta(s_\eta,\mathbf{c})+\tau(s_\eta)} \tag{44}$$

for $\eta = -3 \ldots N_\theta + 3$. For s_η outside the interval $[0,1]$, we assume

$$\left.\frac{\partial \mu}{\partial \theta^\mu}\right|_{\theta(s_\eta,\mathbf{c})+\tau(s_\eta)} = 0$$

this corresponds to a situation in which the spline "hangs loose" outside the limits of the template, being subjected to no attraction.

The system of equations (44) can be written in matrix form as:

$$\mathbf{A}\mathbf{c} = \mathbf{b}(\mathbf{c}) \tag{45}$$

where

$$\begin{aligned} \mathbf{A} &= \{a_{\nu\eta}\} \\ &= \left\{\alpha^2 B_\nu^{(5)}{}_{,4}(s_\eta) - \alpha^1 B_\nu^{(5)}{}_{,2}(s_\eta)\right\},\ \nu = -3 \ldots N_\theta + 3,\ \eta = -3 \ldots N_\theta + 3 \end{aligned} \tag{46}$$

(that is, $A \in \mathbb{R}^{(N_\theta+6)\times(N_\theta+6)}$), and

$$\begin{aligned} \mathbf{b}(\mathbf{c}) &= \{b_\eta(c)\} \\ &= \left\{ \left.\frac{\partial \Psi}{\partial \theta^\mu}\right|_{\theta(s_\eta,\mathbf{c})+\tau(s_\eta)} \right\} \eta = -3 \ldots N_\theta + 3 \end{aligned} \tag{47}$$

(that is, $b \in \mathbb{R}^{(N_\theta+6)}$).

Note that, because of the limited support of the B-spline basis, A is a band matrix with seven nonzero diagonals.

For the solution of (45) we use an iterative technique. Let $c(n)$ be the solution computed at time t, with elements $c_\nu^\mu(n)$. If we consider $\mathbf{b}$ as a constant vector, then the solution of (45) can be (formally) determined as:

$$\mathbf{c} = \mathbf{A}^{-1}\mathbf{b} \tag{48}$$

Since $\mathbf{b}$ is not constant, but depends on the current solution $\mathbf{c}$, this equation must be computed iteratively, until a stable point is reached.

$$\mathbf{c}(n+1) = (1-\varepsilon)\mathbf{c}(n) + \varepsilon \mathbf{A}^{-1}\mathbf{b}(\mathbf{c}(n)) \tag{49}$$

where ε is a suitable learning constant.

6 Measuring the match

Once a numerical solution for the variational problem (9) has been found,, we must provide a measure of how the shape τ and the shape ϕ are similar. This process is quite goal-dependent and, in particular, it depends on whether class assignment or similarity ranking is made.

In this section, we will first discuss match measurement applied to class assignment, and then will discuss the differences for similarity ranking.

In class assignment, we have N_T templates to be matched against one image, and we ask which of the templates ios the closest to the image.

We use capital greek letters to index the different templates, so, τ_Σ is the undeformed version of the Σ-th template, and $\theta^{\Sigma;\mu}$ is the μ-th component ($\mu = 1, 2$) of the Σ-th deformation.

The first quantities we use derive directly from eq. (9). For the Σ-th template, we measure the *Bending energy*:

$$\mathcal{B}^\Sigma = \int_0^1 \left(\theta^{\Sigma;\mu}_{,2}\right)^2 ds \tag{50}$$

the *Strain Energy*:

$$\mathcal{S}^\Sigma = \int_0^1 \left(\theta^{\Sigma;\mu}_{,1}\right)^2 ds \tag{51}$$

and the *Relative matching*:

$$\mathcal{M}^\Sigma = \int_0^1 [\beta(\tau(s) + \theta(s))]^r \, ds \tag{52}$$

The latter measure is called "relative" because it considers all the templates of unitary lenght, and does not measure how much of an image is covered by the template. The measure $\mathcal{M}$ is easier to understand if we think to match the template against the dark areas of the image, i.e. the case in which $\Psi(x) = \beta(x)$. In this case, $\mathcal{M}$ is a measure of how much "gray" there is under the template when the template is considered of unitary lenght. If we think for a moment in terms of binary images, then $\mathcal{M}$ indicates which fraction of the template is on the black area.

This is a limitation of $\mathcal{M}$, as can be seen by observing the situation in Fig. 1. In this case, the template of a "1" is superimposed to the image of a 4. Since all the template is contained in the black area of the image, we have $\mathcal{M} = 1$ in spite of the fact that the "1" template covers only a part of the 4.

In order to discriminate in situations like this, we need another measure that takes into account the fraction of the image that is covered by the template. Since the image is two-dimensional and the template is one-dimensional, this fraction is, strictly speaking, zero. To obtain a meaningful value, consider the distance $\|\cdot\|_2$ in $\mathbb{R}^2$ and, for the deformed template ϕ, the band

$$Q_\rho(\phi) = \left\{ x \in \mathbb{R}^2 \,|\, \min_s \|x - \phi(s)\| \leq \rho \right\} \tag{53}$$

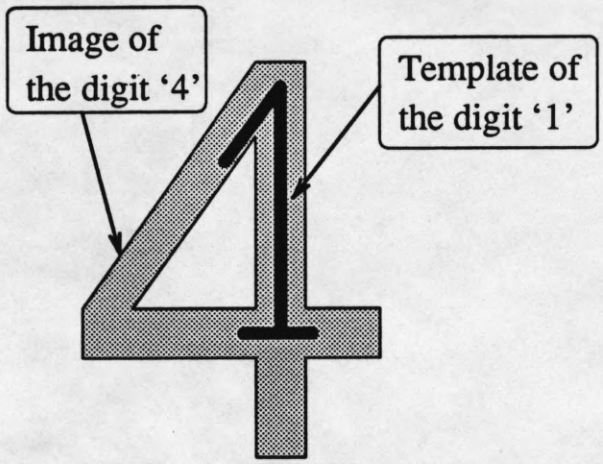

Figure 1: This is a situation in which the measure $\mathcal{M}$ fails. Since the template 1 is completely contained in the black area of the 4, it results $\mathcal{M} = 1$.

around the curve ϕ. The *Absolute matching* is then defined as:

$$\mathcal{A}^{\Sigma} = \int_{Q_{\rho}(\tau^{\Sigma}+\theta^{\Sigma})} \beta(x)dx \tag{54}$$

where the constant ρ is chosen in practice to be rougly the size of a pixel.

The four measures $\mathcal{B}^{\Sigma}$, $\mathcal{S}^{\Sigma}$, $\mathcal{M}^{\Sigma}$, $\mathcal{A}^{\Sigma}$ are used to determine the likelihood that the image is a realization of the template Σ.

We expect the "right" template to have values of $\mathcal{M}^{\Sigma}$ and $\mathcal{A}^{\Sigma}$ higher and values of $\mathcal{B}^{\Sigma}$ and $\mathcal{S}^{\Sigma}$ lower than the other templates, although the exact degree to which this happens depends on the particular application.

These measures make up the base to classify the image. Classification can be done in a number of ways, divided into two broad classes:

The first is *separate classification*, that is, a classifier with four inputs and one output is used for each template. The classifier is given the values $\mathcal{B}^1$, $\mathcal{S}^1$, $\mathcal{M}^1$, and $\mathcal{A}^1$ and yields the likelihood $\mathcal{L}^1$ for the first template, then is given the values $\mathcal{B}^2$, $\mathcal{S}^2$, $\mathcal{M}^2$, and $\mathcal{A}^2$, yielding the likelihood $\mathcal{L}^2$ of the second template, and so on for all the templates. In other words, if C^{sep} is the classification function of the separate classifier, we have (Fig. 2):

$$\mathcal{L}^{\Sigma} = C^{sep}\left(\mathcal{B}^{\Sigma}, \mathcal{S}^{\Sigma}, \mathcal{M}^{\Sigma}, \mathcal{A}^{\Sigma}\right) \tag{55}$$

The second class is a *global classification.* In this case, a single classifier with s many outputs as the number of classes N_C, and $4 \times N_T$ inputs is used. In general, $N_C \leq N_T$, since there may be several temlates belonging to he same class). The output is a vector $\mathcal{G} \in \mathbb{R}^{N_C}$ whose i-th element gives the likelihood that the image is in the i-th class. If C^{glob} is the classification function, and $C^{glob,i}$ its i-th component, then the likelihood that

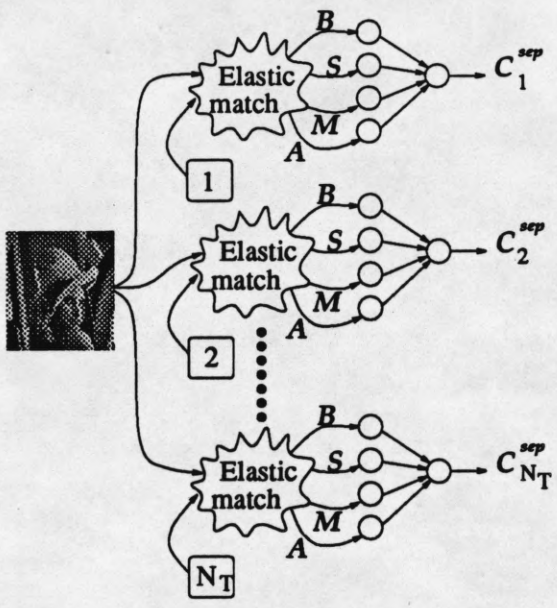

Figure 2: The *separate classifier* solution for the classification of the matching measures. In this case the likelihood measure for the Σ-th template is based on the values $\mathcal{B}^{\Sigma}$, $\mathcal{S}^{\Sigma}$, $\mathcal{M}^{\Sigma}$, $\mathcal{A}^{\Sigma}$ only.

the input image is in the i-th class is:

$$\mathcal{L}_i = C_i^{glob}\left(\mathcal{B}^1, \mathcal{S}^1, \mathcal{M}^1, \mathcal{A}^1, \ldots, \mathcal{B}^{N_T}, \mathcal{S}^{N_T}, \mathcal{M}^{N_T}, \mathcal{A}^{N_T}\right) \tag{56}$$

This arrangement is partially depicted in Fig. 3

Note the slightly different result we obtain from the two systems. In the first case we obtain a likelihood $\mathcal{L}^{\Sigma}$ for every template (whose number is N_T), while in the second case we obtain a likelihood $\mathcal{L}_i$ for every class (whose number is N_C). In the first case, of course, the outcome of the classification will be the class corresponding to the template with the maximum likelihood.

In the case of similarity ranking, there is a single template and a number of images to be matched. Using capital latin letters to index the images, the measures $\mathcal{B}^F$, $\mathcal{S}^F$, $\mathcal{M}^F$ and $\mathcal{A}^F$ can be determined as in the previous case for the F^{th} image.

The *separate classifier* scheme will yield the classification values:

$$\mathcal{L}^F = C^{sep}(\mathcal{B}^F, \mathcal{S}^F, \mathcal{M}^F, \mathcal{A}^F) \tag{57}$$

For most applications of similarity ranking, it is not feasible to have a global classification. For instance, aproblem involving the retrieval from an image database would require a classifier with a number of inputs four times the number of images in the database.

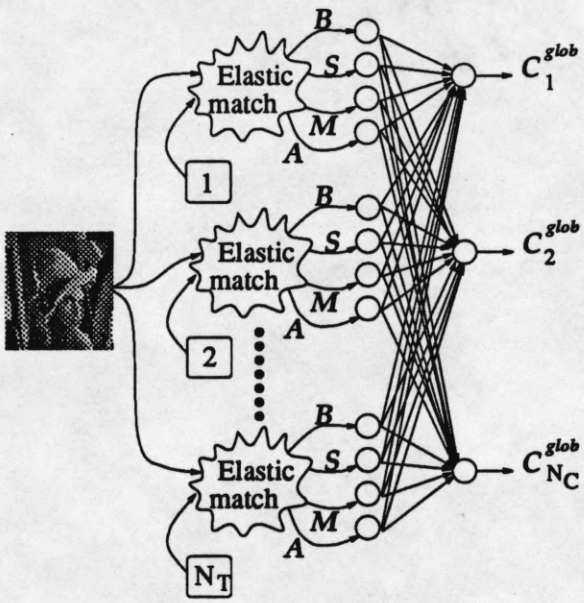

Figure 3: The *global classifier* solution for the classification of the matching measures. In this case the likelihood measure for the i-th class is based on all the $\mathcal{B}$, $\mathcal{S}$, $\mathcal{M}$, and $\mathcal{A}$ values.

7 Dependence on the initial conditions

An important issue to be raised is the dependence of the matching on the initial placement of the template. For most applications, in fact, it is difficult to obtain a precise placement of the template over the pattern to be matched, while a rough placement can be relatively easy to obtain. Therefore, a method that is insensitive to the initial placement of the template is highly desirable.

We carried out a few experiments to gain some insights into this problem by using 89 handwritten digits and 10 digit templates. All the digits were drawn by the same writer. When the correct template was suitably placed above the digit, the convergence was always satisfactory: the template deformed to take into account the differences between the different digits and eventually matched perfectly the digit image.

To investigate the dependence of the matching result on the initial placement of the template, we embedded the digit image (that has dimensions 32×32) in the center of a white "strip" of size 32×96. The size was chosen so that when the template was placed at the extrema of the strip it didn't overlap he image at all.

For each of the 89 digits, the "correct" template – that is, the template corresponding to the digit that had been placed on the strip – was then slided through all the different positions in the strip. At each position, the elastic deformation algorithm was run, and the two matching measures $\mathcal{M}$ and $\mathcal{A}$ were recorded. The two measures were averaged out over all the 89 digits.

Fig. 4 shows how the average $\mathcal{A}$ (upper curve) and the average $\mathcal{M}$ change as a function of the initial position of the template. Both curves have a very similar behavior,

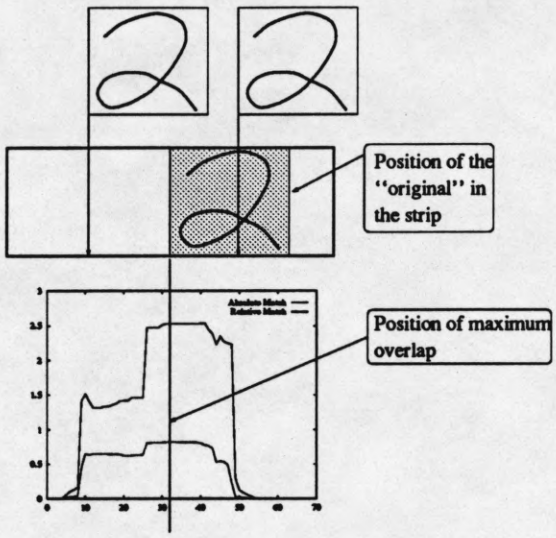

Figure 4: How the match varies with the initial placement of the template

characterized by the presence of two plateaus. The highest plateau surrounds the perfect match position, and corresponds to the placements error that does not have a significant impact over the performances of the method. This can be estimated, in this case, as between 1/3 and 1/2 if the image length. The plateau is not symmetrical around the perfect match point. This is probably due to the fact that most of the digits are also not symmetric. Also, the particular writer we picked up for the experiment, had a slanted calligraphy. This could make it easier for the templates to converge when it is misplaced on one side than on the other.

The region in which we have perfect match extends to templates initially displaced by 1/3 of the image length. This confirms the good position-independence characteristics of the method at least in the case of isolated shapes. This result can be negatively affected by the presence of other shapes close to the shape the template should converge to.

8 OCR by elastic deformation

In this section, we present, as an illustration of the new matching technique, an application to an OCR problem. This is not an attempt to present a complete solution to OCR but to offer some insight in the way the new matching theory could be potentially used to solve a practical problem. This application is quite interesting since the new matching technique avoids one problematic step of OCR applications: the *binarization*, i.e. it is not necessary to convert the original grey-level image data into a binary image.

Most of the current OCR approaches rely on feature extraction and classification. First, a suitable set of features is extracted from the image, then, a classifier is applied to estimate some probability measure for any character, based on the detected features.

The main problem in this approach is that there is no theory to guide the selection

process such a complex case as OCR. To quote [11], pag. 1032:

> .. there is no mathematical principle. Rather it is still an open problem, and there is no sign that it will be solved in the near future. Hence, our intuition has been the most reliable weapon in attacking this problem.

Moreover, most of the structural features (terminal points, loops, joints ...) require a binary image. Therefore, somewhere in the preprocessing stage a bunarization operation to separate the character from the background is necessary. For some images this may not be easy. Consider the image in Fig. 5, which represents a credit card slip obtained by

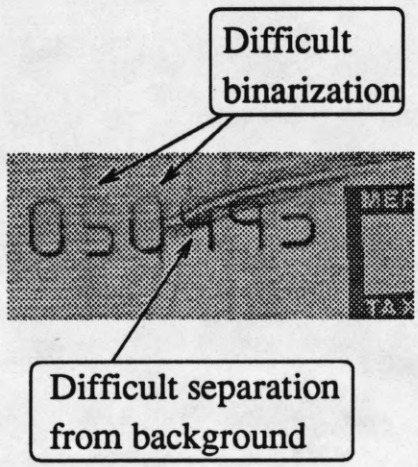

Figure 5: Image of a credit card slip from a receipt carbon copied by a manual machine used to record the purchase. Some of these copies are very dirty because of heavy ink blurring due to the pressure of the moving part of the machine. Binarization can be a hard problem in for this image quality

a manual receipt printer of the type commonly used in shops where no magnetic reader is available. The inprint is obtained by carbon copying the number in relief on the credit card. This procedure causes the ink to blur out the characters and to create a "dirty gray" background, which makes binarization quite difficult. Also, in some cases, like in Fig. 6, although the image is of good quality, separation of the character from the background is extremely difficult because of the background texture present in the slip.

Poor contrast also is a serious problem for attempting to separate individual characters. Most of them are based on connected component analysis ([5]), analysis of the histogram of the image projections, or texture analysis (see [4] for a review of methods).

On the other hand, a new approach to OCR is obtained by fiting the templates directly on the grey level image, avoiding binarization altogether. Moreover, based on the experiments in Sect. 7, elastic template matching is insensitive to reasonable translations, thus allowing the character to be only roughly positioned. The method is also insensitive to small rotations. This allows the system to correctly identify slightly misaligned characters without incurring in the problems caused by excessive invariance as pointed out, for instance, in [10].

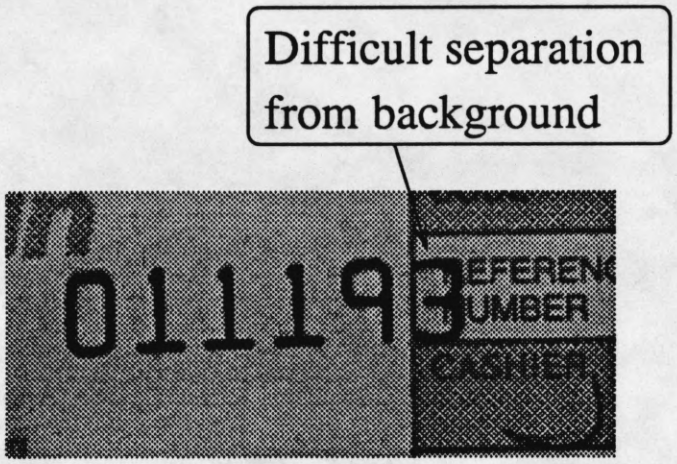

Figure 6: In this case, the inprint (which reports the purchase date) is of good quality, but the background drawing makes quite difficult to separate the digit.

	Digit				
Measure	1	2	3	4	5
$\mathcal{S}$	2.43	2.11	4.43	4.39	3.92
$\mathcal{B}$	1.08	1.26	3.44	2.58	2.22
$\mathcal{A}$	6.21	9.12	8.69	7.22	8.54
$\mathcal{M}$	0.76	0.65	0.67	0.58	0.57
$\mathcal{C}^{sep}$	0.91	1.18	0	0	0
	6	7	8	9	0
$\mathcal{S}$	2.04	5.73	2.67	11.28	2.44
$\mathcal{B}$	1.21	2.39	1.99	2.69	1.41
$\mathcal{A}$	6.59	6.54	11.59	7.51	10.15
$\mathcal{M}$	0.69	0.65	0.60	0.71	0.63
$\mathcal{C}^{sep}$	0.87	0	0.2	0	0.95

8.1 OCR results

In this section, we report results obtained for two different scenarios. In the first test, we try to recognize digits taken from poor quality credit card slips.

Ten digit models are obtained by hand from a good quality sample of credit card digits, and then the ten models are matched against the credit card image data.

Fig. 7 shows the final results obtained by our matching method applied with the ten models. The deformation and match measurements, as well as the classification values obtained by a separate classifier are reported in Tab. 8.1. For this example, the classifier was a simple classifier of the form

$$\mathcal{C}^{sep} = w_1\mathcal{S} + w_2\mathcal{B} + w_3\mathcal{A} + w_4\mathcal{M}$$

where the weights w_i have been trained using the data obtained from 40 good quality

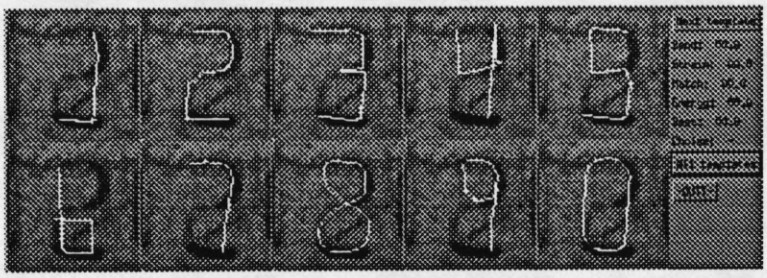

Figure 7: Ten templates deformed to match a digit taken from a credit card slip image

credit card digits.

We also made some experiments in handwritten characters recognition using a subset of the NIST database. The subset is made up of approximately 3,000 characters taken from 50 writers.

We used ten samples (one per digit) from the first of the 50 writers to create the 10 templates to be fitted against the images.

In the first experiment, we attempted *single writer* recognition, that is, we tested the system on all the other digits from the same writer. We used the same simple classification scheme as in the case of the credit card slips. For every template, the four measures $\mathcal{S}$, $\mathcal{B}$, $\mathcal{M}$, and $\mathcal{A}$ were obtained and, based on these, the template was assigned a score given by:

$$S = \mathcal{A} + 2\mathcal{M} - \frac{1}{2}(\mathcal{S} + \mathcal{B}) \tag{58}$$

where the weights have been chosen to roughly balance the differences in relative magnitude of the measures.

After all the scores had been computed, we checked the highest score S_1 and the second highest S_2. The digit was assigned the class of the template that scored S_1. The score S_2 was used to assess the reliability of the classification: if we had

$$\frac{S_1 - S_2}{S_1} \leq 0.05 \tag{59}$$

(i.e. a difference of less than 5% between the highest and the second highest score) the classification was considered as unreliable, otherwise it was considered as reliable.

An example of fitting is reported in Fig. 8. First, we tested the system on the 89

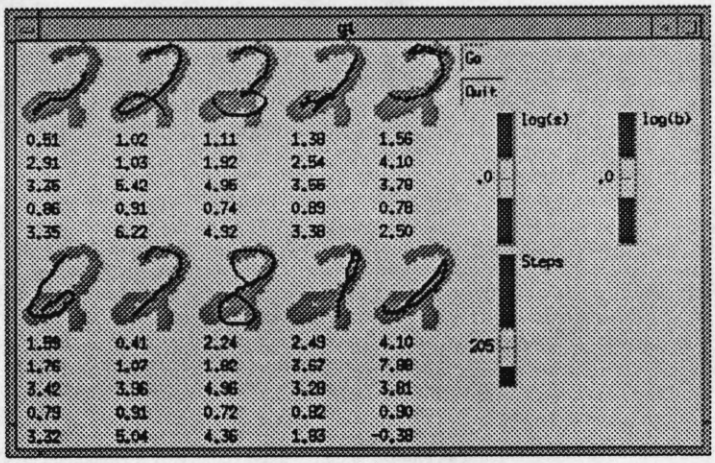

Figure 8: An example of fitting to a sample from the NIST database. The template is obtained from a digit written by the same writer as the test image.

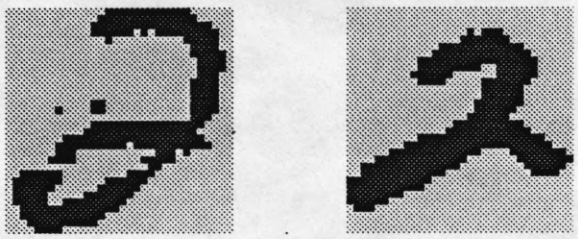

Figure 9: Two instances of the digit 2 found in the NIST database.

digits written by the same writer that produced the templates. We obtained 0% error (no digit was misclassified). In 14 cases, however, the classification was "unreliable". Most of these cases were 1s. We argue that this is because of the exterme similarity between the 1 and the 7, and because of the fact that the simple scoring scheme does not allow for a comparison of the measures relative to these two digits.

When we tested the system on the whole 50 writers set the results were not as good. We obtained a 15% error, and a 17% of unreliably classified digits. In this case, we believe the reason for this poor behavior is in the extremely limited number of templates.

Even with the flexibility provided by the elastic deformation mechanism, a single template per digit is not representative enough to follow the huge variations of style among the 50 writers.

As an example, both digits in Fig. 9 represent a 2, nevertheless, they are very different. Also, some writers close the 4 on the top, while other don't. This result in an extreme variety of shapes that cannot be covered with just one 4 template.

We believe that the flexibility provided by the elastic match will help keeping the number of templates low (well below the number of 1,000 templates reported in [6]).

Further research is being pursued along these directions.

References

[1] P. M. Anselone and P. J. Laurent. A general method for the construction of interpolating or smoothing spline-functions. *Numerische Matematik*, 12:66–82, 1968.

[2] D. J. Burr. A dynamic model for image registration. *Computer Graphics and Image Processing*, 15(2):102–112, 1981.

[3] Larry S. Davis. Shape matching using relaxation techniques. *IEEE Transactions on Pattern Analysis and Machine Intelligence*, 1(1):60–72, 1979.

[4] D. G. Elliman and I. T. Lancaster. A review of segmentation and contextual analysis techniques for text recognition. *Pattern Recognition*, 23(3/4):337–346, 1990.

[5] Hiromichi Fujisawa, Yasuaki Nakano, and Kiyomichi Kurino. Segmentation methods for character recognition: From segmentation to document structure analysis. *Proceedings of the IEEE*, 80(7):1079–1092, July 1992.

[6] Paul Gader, Brian Forester, Margaret Ganzberger, Andrew Gillies, Brian Mitchell, Michael Walken, and Todd Yocum. Recognition of handwritten digits using template and model matching. *Pattern Recognition*, 24(5):421–431, 1991.

[7] Geoffrey E. Hinton, Christopher K. I. Williams, and Michael D. Revow. Adaptive elastic models for hand-printed character recognition. Technical report, Department of Computer Science, University of Toronto, Toronto, Ontario, Canada M5S 1A4, 1992.

[8] Michael Kass, Andrew Witkin, and Demetri Terzopulos. Snakes: Active contour models. *International Journal of Computer Vision*, pages 321–331, 1988.

[9] D. Lovelock and H. Rund. *Tensors, Differential Forms, and Variational Principles.* Dover Books on Advanced Mathematics, 63. Dover Publications, Inc, New York, 1975, 1989.

[10] Yi Lu, Steven Schlosser, and Michael Janeczko. Fourier descriptors and handwritten digit recognition. *Machine Vision and Applications*, 1993. (to appear).

[11] Shunji Mori, Ching Y. Suen, and Kazuro Yamamoto. Historical review of OCR research and development. *Proceedings of the IEEE*, 80(7):1029–1058, July 1992.

[12] T. Okubo. *Differential Geometry.* Monographs and Textbooks in pure and applied mathematics. Marcel Dekker, Inc, 270 Madison Ave. New York 10016, 1987.

[13] Tomaso Poggio, Vincent Torre, and Christof Koch. Computational vision and regularization theory. *Nature*, 317:314–319, September 1985.

[14] Christian H. Reinsch. Smoothing by spline functions. *Numerische Mathematik*, 10:177–183, 1967.

[15] Ramin Samadani. Adaptive snakes: Control of damping and material parameters. In *Proceedings of the SPIE: Geometric Methods in Computer Vision*, volume 1570, pages 202–213, 1991.

[16] A. N. Tihonov. Regularization of incorrectly posed problems. *Soviet Mathematical Doklady*, 4:1624–1627, 1963.

[17] Julian R. Ullman. A use of continuity in character recognition. *IEEE transactions on Systems, Man and Cybernetics*, SMC-4(3):294–300, May 1974.

[18] Debora C. Vargas, Eduardo J. Rodriguez, Myron Flickner, and Jorge L. C. Sanz. Splines and spline fitting revisited. Research Report RJ 8641 (77400), IBM Almaden Research Center, 650 Harry Rd. San Jose, CA 95120-6099, February 1992.

[19] J. B. White and W. J. Welsh. Head boundary location using snakes. *British Telcom Technology Journal*, 8(3):127–136, July 1990.

[20] Christopher K.I. Williams, Michael D. Revow, and Geoffrey E. Hinton. *Hand-Printed Digit Recognition Using Deformable Models.* Cambridge University Press, 1992.